Enhanced photocurrent of a nitride–based photodetector with InN dot-like structures

Lung-Hsing Hsu,[1] Chien-Chung Lin,[2,*] Hau-Vei Han,[3] Da-Wei Lin,[3] Yen-Hua Lo,[2] Yi-Chia Hwang,[2] and Hao-Chung Kuo[3]

[1]*Institute of Lighting and Energy Photonics, National Chiao Tung University, Tainan 711, Taiwan*
[2]*Institute of Photonic System, National Chiao Tung University, Tainan 711, Taiwan*
[3]*Department of Photonic & Institute of Electro-Optical Engineering, National Chiao Tung University, Hsinchu 300, Taiwan*
[*] *chienchunglin@faculty.nctu.edu.tw*

Abstract: The InN dot-like layer was applied in the gallium nitride based material for the purpose of infrared photodetectors (PDs). This InN layer was grown by a low-pressure metal organic chemical vapor deposition technology under different growth temperatures. The X-ray diffraction patterns provide the information of crystal structure and the hexagonal orientation was detected. The Raman shifts and photoluminescence were also used to characterize the quality of InN film. Finally, the fabricated Schottky-type photodetector was tested under a solar simulator and a long-wavelength laser (λ = 1550nm). The measurements show a highly linear relation between photo-generated currents and laser powers for the wavelength of 1550 nm. In the photonic detection range suitable for optical fiber communiation, a quantum efficiency of 9.2% can be observed.

OCIS codes: (040.5160) Photodetectors; (040.3060) Infrared; (250.5230) Photoluminescence; (160.2100) Electro-optical materials; (160.5140) Photoconductive materials.

References and links

1. E. F. Schubert, *Light Emitting Diodes*, 2nd ed. (Cambridge Univ. Press, 2003).
2. S. Nakamura, S. Pearton, and G. Fasol, *The Blue Laser Diode*, 2nd ed. (Springer-Verlag, 2000).
3. C. H. Chiu, P. M. Tu, C. C. Lin, D. W. Lin, Z. Y. Li, K. L. Chuang, J. R. Chang, T. C. Lu, H. W. Zan, C. Y. Chen, H. C. Kuo, S. C. Wang, and C. Y. Chang, "Highly Efficient and Bright LEDs Overgrown on GaN Nanopillar Substrates," IEEE J. Sel. Top. Quantum Electron. **17**(4), 971–978 (2011).
4. S. Nakamura, M. Senoh, S. Nagahama, N. Iwasa, T. Yamada, T. Matsushita, H. Kiyoku, Y. Sugimoto, T. Kozaki, H. Umemoto, M. Sano, and K. Chocho, "InGaN/GaN/AlGaN-based laser diodes with modulation-doped strained-layer superlattices grown on an epitaxially laterally overgrown GaN substrate," Appl. Phys. Lett. **72**(2), 211–213 (1998).
5. H. P. T. Nguyen, Y. L. Chang, I. Shih, and Z. Mi, "InN p-i-n Nanowire Solar Cells on Si," IEEE J. Sel. Top. Quantum Electron. **17**(4), 1062–1069 (2011).
6. C. J. Neufeld, N. G. Toledo, S. C. Cruz, M. Iza, S. P. DenBaars, and U. K. Mishra, "High quantum efficiency InGaN/GaN solar cells with 2.95 eV band gap," Appl. Phys. Lett. **93**(14), 143502 (2008).
7. Y. L. Tsai, C. C. Lin, H. V. Han, C. K. Chang, H. C. Chen, K. J. Chen, W. C. Lai, J. K. Sheu, F. I. Lai, P. Yu, and H. C. Kuo, "Improving efficiency of InGaN/GaN multiple quantum well solar cells using CdS quantum dots and distributed Bragg reflectors," Sol. Energy Mater. Sol. Cells **117**, 531–536 (2013).
8. H. W. Wang, H. C. Chen, Y. A. Chang, C. C. Lin, H. W. Han, M. A. Tasi, H. C. Kuo, P. Yu, and S. H. Lin, "Conversion Efficiency Enhancement of GaN/$In_{0.11}Ga_{0.89}N$ Solar Cells With Nano Patterned Sapphire and Biomimetic Surface Antireflection Process," IEEE Photon. Technol. Lett. **23**(18), 1304–1306 (2011).
9. A. Winden, M. Mikulics, A. Haab, D. Grützmacher, and H. Hardtdegen, "Spectral Sensitivity Tuning of Vertical InN Nanopyramid-Based Photodetectors," Jpn. J. Appl. Phys. **52**(8S), 08JF05 (2013).
10. K. You, H. Jiang, D. Li, X. Sun, H. Song, Y. Chen, Z. Li, G. Miao, and H. Liu, "Shift of responsive peak in GaN-based metal-insulator-semiconductor photodetectors," Appl. Phys. Lett. **100**(12), 121109 (2012).
11. C. H. Chen, K. R. Wang, S. Y. Tsai, H. J. Chien, and S. L. Wu, "Nitride-Based Metal–Semiconductor–Metal Photodetectors with InN/GaN Multiple Nucleation Layers," Jpn. J. Appl. Phys. **49**, 04DG06 (2010).
12. J. Wu, "When group-III nitrides go infrared: New properties and perspectives," J. Appl. Phys. **106**(1), 011101 (2009).
13. J. Wu, W. Walukiewicz, W. Shan, K. M. Yu, J. W. Ager, S. X. Li, E. E. Haller, H. Lu, and W. J. Schaff, "Temperature dependence of the fundamental band gap of InN," J. Appl. Phys. **94**(7), 4457–4460 (2003).
14. T. Matsuoka, H. Okamoto, M. Nakao, H. Harima, and E. Kurimoto, "Optical bandgap energy of wurtzite InN," Appl. Phys. Lett. **81**(7), 1246–1248 (2002).

#223574 - $15.00 USD Received 22 Sep 2014; revised 5 Nov 2014; accepted 7 Nov 2014; published 17 Nov 2014

15. L. Guo, X. Wang, L. Feng, X. Zheng, G. Chen, X. Yang, F. Xu, N. Tang, L. Lu, W. Ge, and B. Shen, "Temperature sensitive photoconductivity observed in InN layers," Appl. Phys. Lett. **102**(7), 072103 (2013).
16. H. Sekiguchi, K. Kishino, and A. Kikuchi, "Emission color control from blue to red with nanocolumn diameter of InGaN/GaN nanocolumn arrays grown on same substrate," Appl. Phys. Lett. **96**(23), 231104 (2010).
17. H. P. T. Nguyen, K. Cui, S. Zhang, M. Djavid, A. Korinek, G. A. Botton, and Z. Mi, "Controlling Electron Overflow in Phosphor-Free Ingan/Gan Nanowire White Light-Emitting Diodes," Nano Lett. **12**(3), 1317–1323 (2012).
18. J. Park, H. Ryu, T. Son, and S. Yeon, "Epitaxial Growth of ZnO/InN Core/Shell Nanostructures for Solar Cell Applications," Appl. Phys. Express **5**(10), 101201 (2012).
19. K. M. Yu, Z. Liliental-Weber, W. Walukiewicz, W. Shan, J. W. Ager, S. X. Li, R. E. Jones, E. E. Haller, H. Lu, and W. J. Schaff, "On the crystalline structure, stoichiometry and band gap of InN thin films," Appl. Phys. Lett. **86**(7), 0719110 (2005).
20. A. G. Bhuiyan, A. Hashimoto, and A. Yamamoto, "Indium nitride (InN): A review on growth, characterization, and properties," J. Appl. Phys. **94**(5), 2779–2808 (2003).
21. S. Ruffenach, B. Maleyre, O. Briot, and B. Gil, "Growth of InN quantum dots by MOVPE," Phys. Status Solidi **2**(2), 826–832 (2005).
22. W. C. Ke, C. P. Fu, C. Y. Chen, L. Lee, C. S. Ku, W. C. Chou, W.-H. Chang, M. C. Lee, W. K. Chen, W. J. Lin, and Y. C. Cheng, "Photoluminescence properties of self-assembled InN dots embedded in GaN grown by metal organic vapor phase epitaxy," Appl. Phys. Lett. **88**(19), 191913 (2006).
23. O. Briot, S. Ruffenach, M. Moret, B. Gil, C. Giesen, M. Heuken, S. Rushworth, T. Leese, and M. Succi, "Growth of InN films and nanostructures by MOVPE," J. Cryst. Growth **311**(10), 2761–2766 (2009).
24. B. Maleyre, O. Briot, and S. Ruffenach, "MOVPE growth of InN films and quantum dots," J. Cryst. Growth **269**(1), 15–21 (2004).
25. A. Luque and A. Marti, "Increasing the efficiency of ideal solar cells by photon induced transitions at intermediate levels," Phys. Rev. Lett. **78**(26), 5014–5017 (1997).
26. C. C. Lin, M. H. Tan, C. P. Tsai, K. Y. Chuang, and T. S. Lay, "Numerical study of quantum-dot-embedded solar cells," IEEE J. Sel. Top. Quantum Electron. **19**, 4000110 (2013).
27. V. J. Gómez, P. E. D. Soto Rodriguez, P. Kumar, E. Calleja, and R. Nötzel, "High In Composition InGaN for InN Quantum Dot Intermediate Band Solar Cells," Jpn. J. Appl. Phys. **52**(8S), 08JH09 (2013).
28. P. Bhattacharya, S. Ghosh, and A. D. Stiff-Roberts, "Quantum Dot Opto-Electronic Devices," Annu. Rev. Mater. Res. **34**(1), 1–40 (2004).
29. J. Shao, T. E. Vandervelde, A. Barve, A. Stintz, and S. Krishna, "Increased normal incidence photocurrent in quantum dot infrared photodetectors," Appl. Phys. Lett. **101**(24), 241114 (2012).
30. D. I. Son, H. Y. Yang, T. W. Kim, and W. I. Park, "Photoresponse mechanisms of ultraviolet photodetectors based on colloidal ZnO quantum dot-graphene nanocomposites," Appl. Phys. Lett. **102**(2), 021105 (2013).
31. E. J. Miller, E. T. Yu, P. Waltereit, and J. S. Speck, "Analysis of reverse-bias leakage current mechanisms in GaN grown by molecular-beam epitaxy," Appl. Phys. Lett. **84**(4), 535–537 (2004).
32. W. Huang, M. Yoshimoto, K. Taguchi, H. Harima, and J. Saraie, "Improved Electrical Properties of InN by High-Temperature Annealing with In Situ Capped SiNx Layers," Jpn. J. Appl. Phys. **43**(1A/B), L97–L99 (2004).
33. J. W. Ager, N. Miller, R. E. Jones, K. M. Yu, J. Wu, W. J. Schaff, and W. Walukiewicz, "Mg-doped InN and InGaN – Photoluminescence, capacitance–voltage and thermopower measurements," Phys. Status Solidi **245**(5), 873–877 (2008).
34. T. Fujii, A. Kobayashi, K. Shimomoto, J. Ohta, M. Oshima, and H. Fujioka, "Structural Characteristics of GaN/InN Heterointerfaces Fabricated at Low Temperatures by Pulsed Laser Deposition," Appl. Phys. Express **3**(2), 021003 (2010).
35. C. Y. Chen, L. Lee, S. K. Tai, S. F. Fu, W. C. Ke, W. C. Chou, W. H. Chang, M. C. Lee, and W. K. Chen, "Optical Properties of Uncapped InN Nanodots Grown at Various Temperatures," Jpn. J. Appl. Phys. **48**(3), 031001 (2009).
36. F. Ivaldi, C. Meissner, J. Domagala, S. Kret, M. Pristovsek, M. Högele, and M. Kneissl, "Influence of a GaN Cap Layer on the Morphology and the Physical Properties of Embedded Self-Organized InN Quantum Dots on GaN(0001) Grown by Metal–Organic Vapor Phase Epitaxy," Jpn. J. Appl. Phys. **50**(3R), 031004 (2011).
37. I. Shalish, G. Seryogin, W. Yi, J. M. Bao, M. A. Zimmler, E. Likovich, D. C. Bell, F. Capasso, and V. Narayanamurti, "Epitaxial catalyst-free growth of InN nanorods on c-plane sapphire," Nanoscale Res. Lett. **4**(6), 532–537 (2009).
38. M. Jamil, R. A. Arif, Y.-K. Ee, H. Tong, J. B. Higgins, and N. Tansu, "MOVPE of InN films on GaN templates grown on sapphire and silicon(111) substrates," Phys. Status Solidi A **205**(7), 1619–1624 (2008).
39. Y. K. Fu, C. H. Kuo, C. J. Tun, C. W. Kuo, W. C. Lai, G. C. Chi, C. J. Pan, M. C. Chen, H. F. Hong, and S. M. Lan, "Self-assembled InN dots grown on GaN with an $In_{0.08}Ga_{0.92}N$ intermediate layer by metal organic chemical vapor deposition," J. Cryst. Growth **310**(20), 4456–4459 (2008).
40. R. Singh, D. Doppalapudi, T. D. Moustakas, and L. T. Romano, "Phase separation in InGaN thick films and formation of InGaN/GaN double heterostructures in the entire alloy composition," Appl. Phys. Lett. **70**(9), 1089–1091 (1997).
41. C. H. Jia, Y. H. Chen, X. L. Zhou, G. H. Liu, Y. Guo, X. L. Liu, Y. S. Yang, and Z. G. Wang, "InN layers grown by MOCVD on SrTiO3 substrates," J. Cryst. Growth **312**(3), 373–377 (2010).
42. O. Briot, B. Maleyre, S. Ruffenach, B. Gil, C. Pinquier, F. Demangeot, and J. Frandon, "Absorption and Raman scattering processes in InN films and dots," J. Cryst. Growth **269**(1), 22–28 (2004).

#223574 - $15.00 USD Received 22 Sep 2014; revised 5 Nov 2014; accepted 7 Nov 2014; published 17 Nov 2014

43. S. Hernández, R. Cuscó, D. Pastor, L. Artús, K. P. O'Donnell, R. W. Martin, I. M. Watson, Y. Nanishi, and E. Calleja, "Raman-scattering study of the InGaN alloy over the whole composition range," J. Appl. Phys. **98**(1), 013511 (2005).
44. V. Y. Davydov, A. A. Klochikhin, V. V. Emtsev, A. N. Smirnov, I. N. Goncharuk, A. V. Sakharov, D. A. Kurdyukov, M. V. Baidakova, V. A. Vekshin, S. V. Ivanov, J. Aderhold, J. Graul, A. Hashimoto, and A. Yamamoto, "Photoluminescence and Raman study of hexagonal InN and In-rich InGaN alloys," Phys. Status Solidi **240**(2), 425–428 (2003).
45. J. W. Chen, Y. F. Chen, H. Lu, and W. J. Schaff, "Cross-sectional Raman spectra of InN epifilms," Appl. Phys. Lett. **87**(4), 041907 (2005).
46. E. Munoz Merino, E. Monroy, F. Calle, M. A. Sanchez, E. Calleja, F. Omnes, P. J. L. Gibart, F. Jaque, and I. Aguirre de Carcer, "AlGaN-based photodetectors for solar UV applications," Proc. SPIE **3629**, 200–210 (1999).
47. S. Assefa, F. Xia, S. W. Bedell, Y. Zhang, T. Topuria, P. M. Rice, and Y. A. Vlasov, "CMOS-integrated high-speed MSM germanium waveguide photodetector," Opt. Express **18**(5), 4986–4999 (2010).
48. M. Nakano, T. Makino, A. Tsukazaki, K. Ueno, A. Ohtomo, T. Fukumura, H. Yuji, S. Akasaka, K. Tamura, K. Nakahara, T. Tanabe, A. Kamisawa, and M. Kawasaki, "Transparent polymer Schottky contact for a high performance visible-blind ultraviolet photodiode based on ZnO," Appl. Phys. Lett. **93**(12), 123309 (2008).

1. Introduction

In recent years, nitride–based alloys, such as AlN, GaN and InN etc, have achieved great success in light emitting diodes [1–3], laser diodes [4], solar cells [5–8], and photodetectors [9–11]. In these works, most of them focused on the visible wavelength range which are inherent to InGaN/GaN materials. Meanwhile, one of the great features about nitride-based materials is the wide direct bandgap coverage associated with the compositional variation, which ranges from 0.7 eV for InN to 3.4 eV for GaN, and thus provides a wide range of the absorption spectrum from ultraviolet to visible and infrared [12–15]. However, to date, the epitaxial layer with high-In composition or pure InN is still difficult to be accomplished. The high quality epitaxial InN film cannot be achieved easily on native sapphire or GaN surface due to the large mismatch in lattice constant (10.78% in the c-axis GaN) [12,16–20]. In the past, molecular beam epitaxy (MBE) has been a major technique for InN growth, both 2D and 3D (Stransky–Krastanov, or SK) mode has been reported [20]. However, due to huge differences of the equilibrium vapor pressure in MOCVD system for AlN/GaN and InN, InN is extremely difficult to grow a nice mirror-like thin film unless the V/III ratio raised beyond unreasonable number of 8×10^4 [20]. Thus in many cases, the 3D (SK) growth mode becomes more preferrable for InN [21–24]. In addition to alleviate the aforementioned material issue, the other benefit of nano-scale structure also includes the introduction of intermediate band (IB), and several groups also have demonstrated extra light-absorption through this IB effect in quantum dots (QDs) [25,26], and the solar cell application of the IB concept with InN quantum dot has also been previously proposed [27]. Previously, the quantum dot design was applied to PDs for improvement in the optoelectronic characteristics of devices and enhancement of the internal quantum efficiency (IQE) [28–30]. However, the reverse-bias leakage current due to dislocations in the high-In content layer is still yet to be overcome [31].

In this study, we employed a low-pressure metal organic chemical vapor deposition (MOCVD) technology to grow an InN dot-like structures on regular GaN material for photodetector purpose. The extended InN photoluminescence can be observed in cryogenic and room temperature. Further X-ray measurement confirmed the Wurtzite configuration of these dot-like structure. The 1550nm laser excitation measurement of the device's photo-current provide us the responsivity of the material. From various growth conditions and their characterizations, the best growth temperature can be estimated in our system. We believe this InN dot-like design could be essential for the nitride based material to further extend their usage to infrared photodetection.

#223574 - $15.00 USD Received 22 Sep 2014; revised 5 Nov 2014; accepted 7 Nov 2014; published 17 Nov 2014

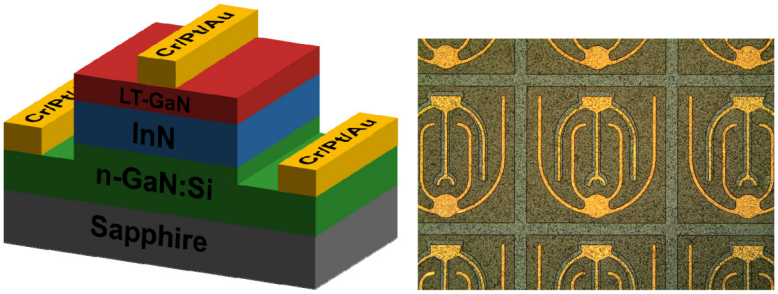

(a) (b)

Fig. 1. (a) Schematic of the nitride-based photodetector with InN dot-like structures. (b) The microscopic image of a finished device under test.

2. Experiments

All the nitride-based layers, including InN dot-like structures, were grown on c-plane sapphire substrates by a Veeco D75 MOCVD system. On the sapphire substrate, the nitride- based structure consists of a 30-nm-thick low-temperature GaN nucleation layer, a 1.5-μm-thick undoped GaN epilayer, a 2-μm-thick Si-doped GaN epilayer (n-GaN:Si), followed by 65-nm-thick InN epilayer, and then a 100-nm-thick low-temperature GaN epilayer (LT-GaN) with the same growth temperature as the previous InN layer was capped on the top. The functionality of LT GaN layer is three-fold: first, protection for subsequent thermal cycling [32], a better contact layer with less electron affinity (4.1eV vs. 5.8 eV of InN [33]), and finally, a clean interface for better carrier transport [34]. After the epitaxial growth, a Cr/Pt/Au (5nm/5nm/190nm) alloy contact pads were applied to the bottom side for n-GaN and top contacts by photolithography and lift-off process steps. The mesa was defined by dry-etch with the size of 14 mil by 14 mil (355μm by 355μm). The schematic diagram of the finished device is depicted in Fig. 1. In addition, a wafer without the LT-GaN capping layer was also grown for comparison. During the growth, trimethylgallium (TMGa), trimethylindium (TMIn), and ammonia (NH_3) were employed as the reactant source elements for gallium, indium, and nitrogen sources, respectively. Silane was used as the source for n-type dopants. For the growth of InN-dot structures, flow rates of TMIn and NH_3 were fixed at 130 sccm and 7000 sccm, respectively, during the InN-dots formation process. The doping concentration of Si-doped GaN layer is 4.5×10^{18} cm^{-3}. After the growth of InN layer, the samples were characterized using field-emission scanning electron microscopy (SEM), energy dispersive spectrometer (EDS) taken by a JEOL ARM-200F system, high resolution X-ray diffraction (HRXRD), photoluminescence (PL) using the 633 nm line of a He-Ne laser as the excitation source, the high resolution confocal Raman scattering (Raman) system and the spectrophotometer ranging from UV to visible wavelength (UV-VIS). Finally, after normal clean-room processes are finished, the device performance was first measured by a Newport 1000W Class-A AM1.5G solar spectrum system. A tunable DFB laser source (in the 1550 nm range) and current-voltage (I-V) system were also employed to evaluate external quantum efficiency for photoresponsivity purpose.

#223574 - $15.00 USD Received 22 Sep 2014; revised 5 Nov 2014; accepted 7 Nov 2014; published 17 Nov 2014

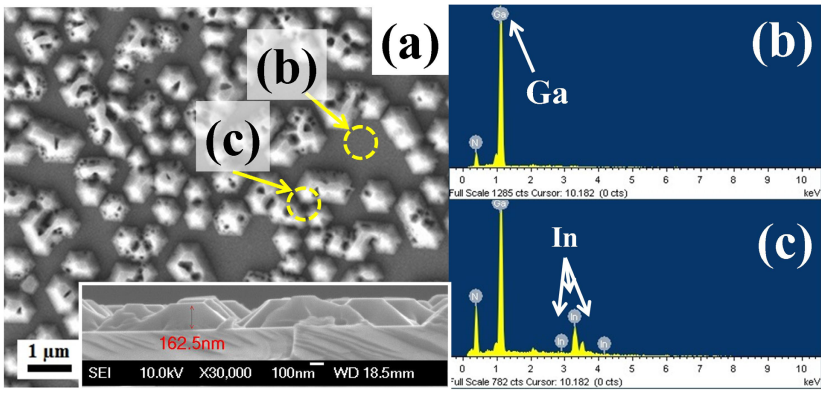

Fig. 2. (a) Top-view SEM image of InN dot-like on the n-GaN:Si substrate. The (b) and (c) symbols indicate the different measured area on the sample. The inset SEM image is the cross-sectional view of the InN dot-like structure with the marked height of 162.5nm. (b) and (c) are the energy dispersive spectrometer (EDS) data from marked area of Fig. 2(a).

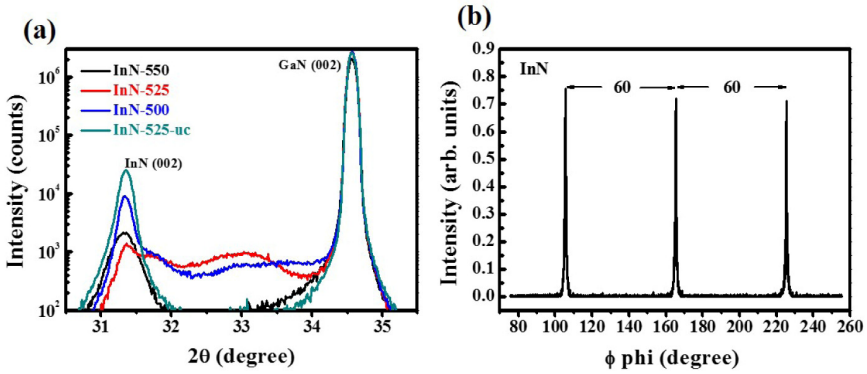

Fig. 3. The HRXRD patterns: (a) 2θ scan of samples with various growth temperatures and (b) φ scan of 525°C uncapped wafer.

3. Results and discussion

First thing to be characterized is whether indium was incorporated into the layer. Indium is notorious for evaporating easily at low temperature, and the remaining poor quality materials are left on the substrate. To find out the best condition for our MOCVD system, four samples of InN-dots with different growth temperature (500, 525, 550 degrees Celsius) on n-GaN:Si substrate with/without a LT-GaN capping layer, were fabricated for characterization: (1) 500°C (InN-500), (2) 525°C (InN-525), (3) 550°C (InN-550), and (4) 525°C without LT-GaN (InN-525-uc).

Figure 2 shows SEM and Energy Dispersion Spectrometer (EDS) measurement results of InN-dots layer with growth temperature of 525°C. The top-view SEM image reveals that the diameters of InN dot-like structures are between 300 nm and 700 nm and the height is around 162.5 nm, as shown in the inset of Fig. 2(a). From different areas in Fig. 2(a), EDS signals can be extracted and shown in Fig. 2(b) and (c). The flat area does not bear any sign of indium (Fig. 2(b)), while the island area demonstrates clear indium incorporation (Fig. 2(c)). On the other hand, several islands tend to merge together due to self-assemble effect [24,35,36], and voids also show up at the center of In-rich islands.

Once we confirm the In content is presented in the low-temperature film, other tests such as high-resolution X-ray diffraction (HRXRD) can be performed. Figure 3(a) exhibits HRXRD results of InN epitaxy with various growth temperatures. The peaks of all samples

#223574 - $15.00 USD Received 22 Sep 2014; revised 5 Nov 2014; accepted 7 Nov 2014; published 17 Nov 2014

centered at 2θ = 31.3° and 34.56° corresponded to the diffraction of the hexagonal phase InN (0002) [20,37,38] and GaN (0002) plane, respectively. In addition to the diffraction peak of InN (0002) and GaN (0002) plane, the other broad-band peak at 2θ = 33.2° originated from the diffraction of polycrystalline InN was observed [19,39]. We believe that this broad-band signal indicates possible disorder in the crystal structure and possible InGaN alloy formation in the film, which lower the XRD intensity of the main InN peak and smear the signal in between InN and GaN [40]. In general, the InN signal is enhanced when the growth temperature is getting lower, and strongest at InN-525-uc (the uncapped sample). Compared between the 525°C samples, the LT-GaN capping layer seems to deteriorate the quality of previously deposited InN material by providing Ga source for inter-mixing and alloying InGaN composite. A wider range scan in the planar direction (φ-direction) produces a series of signal separated by 60 degrees which can be a good indicator of hexagonal crystal structure of InN dot-like region [41].

Figure 4 shows the Raman spectrum at room temperature observed from the grown surface using the He-Ne laser at 632.8 nm. As seen in the figure, a sharp phonon signal (E_2-high frequency mode) from the n-GaN:Si substrate at 567 cm^{-1} (E_2 GaN) and the phonon longitudinal optical modes (A_1LO GaN) at 733 cm^{-1} can be expected. The signature of the indium nitride material exhibits through A_1LO InN (longitudinal optical modes) at 594 cm^{-1} and E_2 InN at 490 cm^{-1} (high frequency mode). The observation of A_1LO InN at 594 cm^{-1} indicates a low carrier density region in InN materials and generally implies a good epitaxial quality [14]. In our samples, InN-525-uc seems to have better InN quality than others with LT-GaN capping layer by demonstrating several key InN signals. The A_1LO peak intensity of InN-550 is weak, when compared to other samples with lower growth temperature. Previously, A_1LO Raman peak shift of the InN film was correlated to InN-dots size [42]. There are two big shoulders peaked at 680cm^{-1} for the samples of InN-500 and InN-525. These peaks are believed to be the InGaN alloy formed during the subsequent GaN capping growth. The intermixing between the indium and gallium elements can be examined via the TEM and EDS experiments later. The location of the peaks is directly related to composition of the InGaN alloy, which is $In_{0.6}Ga_{0.4}N$ in this case, while the line width is broadened by the elastic scattering of LO phonons due to compositional fluctuations [43,44]. The slight redshift of E_2(high) mode of InN-550 sample could be attributed to the residual strain developed during the cooling cycle. The difference between the thermal expansion coefficients of GaN and InN can leave the grown InN structure under tensile strain, which can move the Raman peak towards lower frequency [45].

The photoluminescence (PL) was measured using the 633 nm line of a He-Ne laser as the excitation source. Two different samples were measured for their PL characteristics. Figure 5 shows the power-dependent PL spectra of InN-525 and InN-525-uc measured at 10 K. The PL spectra of InN-525 exhibits multiple peaks energy centered at 0.75, 0.83, and 0.92 eV, and meanwhile InN-525-uc also exhibits multiple peaks energy centered at 0.72 and 0.74 eV, respectively. The blue shift of PL peaks of InN-525 can be observed in Fig. 5(b). The cause of this shift can be attributed to the possible diffusion of Ga in the final GaN capping growth and the loss of pure InN material [22]. From the TEM cross-section view and the corresponding EDS analysis, shown in Fig. 6(a) and (b), distinctive Ga and In signals can be found both in InN and GaN cap layers, while no In signal can be seen in the GaN substrate. The EDS line-scan in our scanning transmission electron microscope (STEM) can provide the elemental depth profiles shown in Fig. 6(c). The meaured layer thickness is thinner because the cross-section happened to be at the tail of the InN dot structure which can also be seen from the boundary of the TEM image in Fig. 6(a). The excess Ga intensity with the In signal in the same location can be seen as another evidence for Ga diffusion. Combined with previous X-ray and Raman data, the inter-mixing of GaN and InN during the capping growth is confirmed. Compared with InN-525-uc, the PL intensity of the InN-525 sample is also weaker. It is possible that extra damage of InN film is caused during the capping layer growth and leads to worse PL spectra.

#223574 - $15.00 USD Received 22 Sep 2014; revised 5 Nov 2014; accepted 7 Nov 2014; published 17 Nov 2014

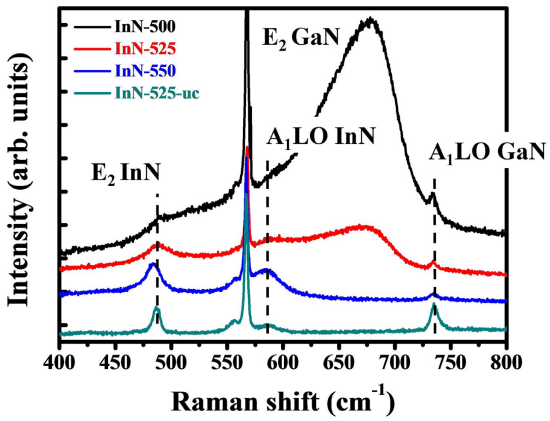

Fig. 4. Raman spectrum for InN dots grown with different growth temperature on the n-GaN:Si substrate.

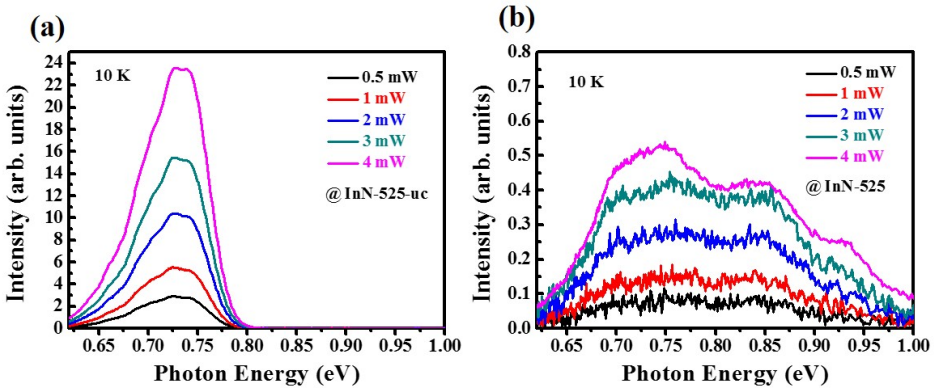

Fig. 5. (a) The photoluminescence spectra at 10 K for InN-525-uc structures without LT-GaN and (b) with a capping LT-GaN layer.

Finally the detector chip can be measured under various conditions. Because of our special layer structure design (without p-GaN on the top contacting layer), this device is more like a Schottky-junction type of photodetector. Figure 7(a) shows the photovoltaic response under AM1.5G solar simulator for various growth temperatures. The ratio of photo current to dark current is extracted for the comparison. From the measured results, an increasing trend of the photo/dark ratio with the growth temperature is obtained. This can be attributed to the better quality of the GaN growth, not the InN layer, in the device due to higher temperature. Meanwhile, a limited improvement of the photo/dark ratio of InN-525-uc over that of InN-525 is probably due to less defects in the film. To really identify the functionality of InN, it is better to use a long-wavelength light source to examine the devices because long-wavelength photons don't get absorbed by GaN. A 1550nm tunable DFB laser was used to illuminate the sample and negative bias was applied to the device. Both dark current and photocurrent under various laser powers can be recorded. The measured photo-generated currents and laser powers were converted such that the quantum efficiency (defined by # of electron-hole pairs/# of the photons) can be evaluated. All devices but InN-525 samples exhibit negative photo-conductivities under increasing laser power, which could be explained as extra recombination centers or existing donor states in the band gap in the InN films [15]. The performance of the best InN-525 device, as seen in Fig. 7(b) and (c), exhibits good reverse bias IV up to −0.3V under laser illumination, and the photocurrent versus laser power at 1550nm is 0.443 A/W. When it is compared to the dark current in Fig. 7(b), the photo-generated current takes as high

#223574 - $15.00 USD Received 22 Sep 2014; revised 5 Nov 2014; accepted 7 Nov 2014; published 17 Nov 2014

as 27.7% of the dark current, which marks a significant increment suitable for photo-detection. The linear extrapolation of the measured photocurrent response in Fig. 7(c) exhibit certain “threshold” power needed to initiate the photocurrent extraction. This phenomenon has been documented previously [46–48], and we believe the excess traps and defects between the InN and GaN are the most possible reason to consume the excitation laser photons at the low input power level. Figure 7(d) shows the resultant spectral response of this InN photodetector at the reverse bias of 0.3 Volts. The tuning range of the DFB laser limits our data acquisition, and an external quantum efficiency as high as 9.2% is recorded.

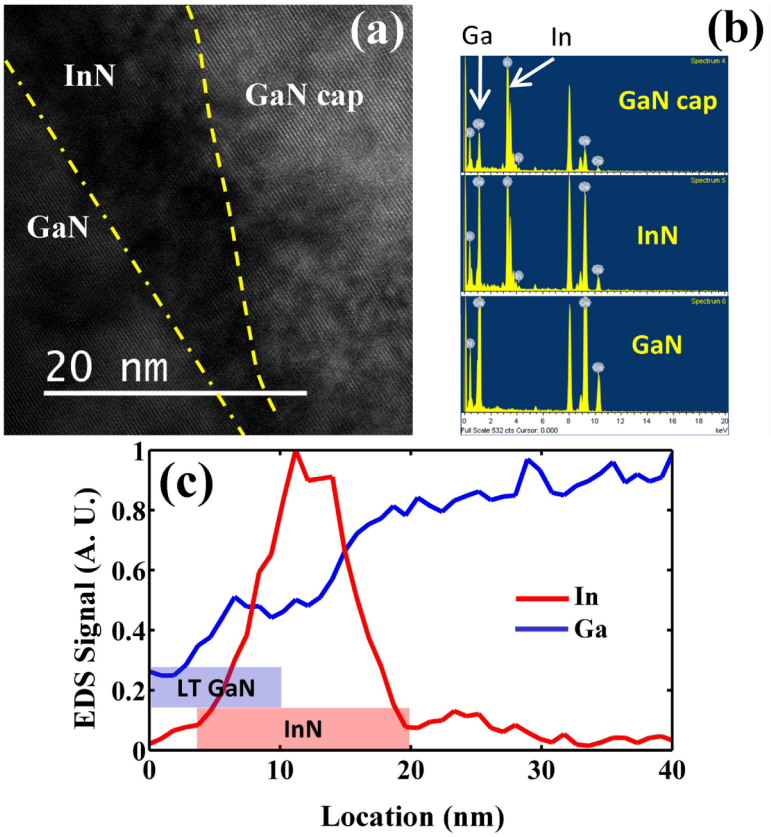

Fig. 6. (a) The TEM of the GaN cap/InN/GaN substrate. The dash line is the rough boundary between these layers and for eye-guiding only. (b) The EDS plots are shown for different regions of the structure. (c) The EDS line-scan results vs. location for indium and gallium concentration. The blue and red stripes at the bottom of the plot indicate the approximate range of InN and LT GaN layers. The highly overlapped section should result from the Ga diffusion.

#223574 - $15.00 USD Received 22 Sep 2014; revised 5 Nov 2014; accepted 7 Nov 2014; published 17 Nov 2014

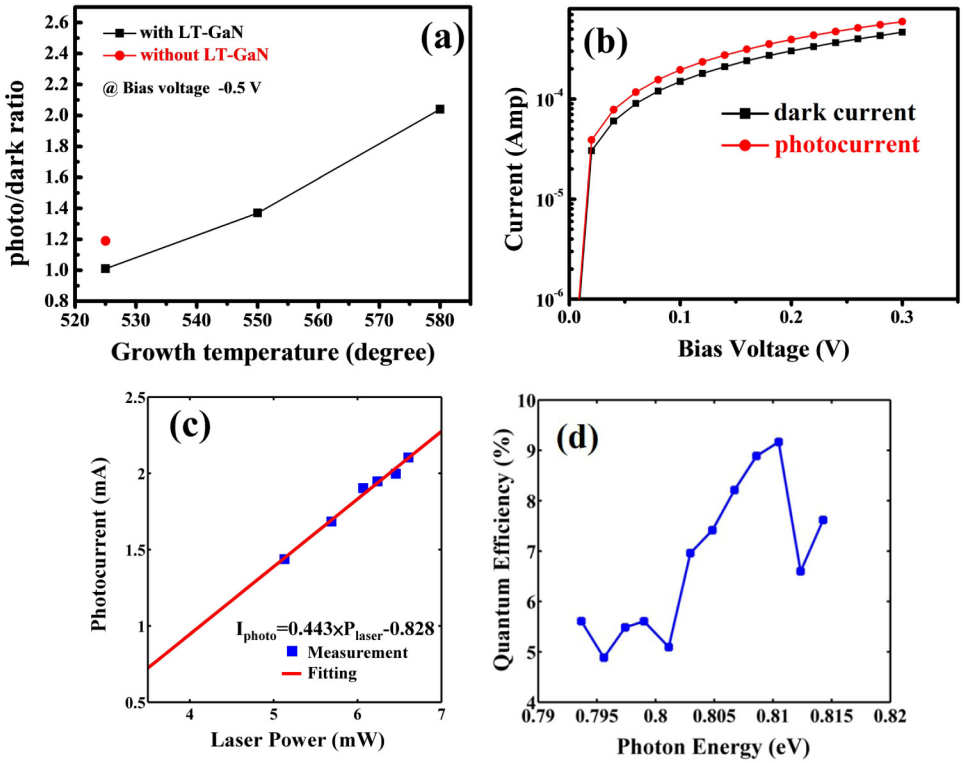

Fig. 7. (a) The ratio of photocurrent to dark current at reverse-bias corresponding to InN growth temperature of 525, 550, and 580 °C, and the comparison with InN-525-uc. (b) The reverse-bias I-V characteristics of the InN-525 measured in dark and under illumination of 1550 nm DFB laser light. (c) The reverse biased current (substracted by dark current) under various pump laser power. The reverse bias is –0.2V in the plot, and the linear slope of 0.443 (A/W) can be fitted from the measured data. (d) The external quantum efficiency of the InN photodetector between 0.79eV and 0.815eV.

4. Conclusion

In summary, we successfully grew InN-dot like structures by MOCVD system and utilized this structure to fabricate a photodetector. The suitable growth temperature of InN dot-like structures can be found via various material characterizations, and at current stage, a low-temperature capping layer of GaN seems not favorable for InN formation. With the help of both the solar simulator and the long-wavelength laser, the photodetection capability of the InN device is fully explored and a highly linear photo-current vs. input power relation can be found from the sample of 525°C growth temperature with GaN capping. Finally the spectral responsivity and thus the quantum efficiency can be measured by the tunable DFB laser excitation, and the best efficiency is 9.2%. We believe this structures shall be promising to be integrated in the future generation of nitride-based optoelectronic devices.

Acknowledgment

The authors would like to thank the supports of Advanced Optoelectronic Technology Inc. The work was supported by the National Science Council of Taiwan through the contracts: NSC 101-2221-E-009-046-MY3 and MOST103-2120-M-110-003.

#223574 - $15.00 USD Received 22 Sep 2014; revised 5 Nov 2014; accepted 7 Nov 2014; published 17 Nov 2014